Physica C 202 (1992) 1–11
North-Holland

PHYSICA C

Growth and relaxation mechanisms of $YBa_2Cu_3O_{7-x}$ films

S.J. Pennycook [a], M.F. Chisholm [a], D.E. Jesson [a], R. Feenstra [a], S. Zhu [a,1], X.Y. Zheng [b,1] and D.J. Lowndes [a]

[a] *Solid State Division, Oak Ridge National Laboratory, Oak Ridge, TN 37831, USA*
[b] *Health and Safety Research Division, P.O. Box 2008, Oak Ridge, TN 37831, USA*

Received 4 August 1992

Using a combination of *Z*-contrast scanning transmission electron microscopy, scanning tunneling microscopy, and plan view diffraction contrast imaging, we have studied the growth and relaxation mechanisms of $YBa_2Cu_3O_{7-x}$ deposited on MgO and $SrTiO_3$ substrates. Two-dimensional island growth occurs on $SrTiO_3$ substrates, with relaxation through the nucleation of dislocation half-loops. The threading dislocation segments then have a screw component and can lead to kinetic roughening through the development of growth pyramids. In contrast, growth on MgO occurs by true three-dimensional island growth (with no wetting layer), most of the interface being incommensurate with the substrate (although crystallographically aligned). Dislocations with both edge and screw components are generated on island coalescence. A highly anisotropic surface energy is shown to be responsible for cell-by-cell $c\perp$ growth being thermodynamically preferred, although at high supersaturations a transition to $a\perp$ growth occurs.

1. Introduction

The growth mechanisms of the layered superconductors, like their transport properties, are highly anisotropic. Equally importantly, deposition, whether by laser ablation, sputtering, or molecular beam epitaxy (MBE), can take place very far from equilibrium, and microstructures may well be determined by kinetic factors rather than thermodynamics. The competition between kinetics and thermodynamics plays an important role in determining surface morphology, which translates into interface morphology in superlattices and device structures, therefore determining the eventual transport characteristics. There is much current interest, therefore, in the link between growth mechanisms and microstructures [1–8].

Using the new technique of *Z*-contrast imaging in the scanning transmission electron microscope (STEM), the interface morphology and hence the growth mechanism can be visualized directly. We have also used scanning tunneling microscopy (STM) and plan view transmission electron microscopy (TEM) to study the initial stages of film growth, the density of threading edge and screw dislocations, and their nucleation mechanisms. Even though the final morphology of films grown on $SrTiO_3$ and MgO is very similar, the development of the microstructures, and the origin and density of the threading dislocations, is completely different. In particular we find that cell-by-cell $c\perp$ growth is thermodynamically preferred, but that whether two- or three-dimensional growth occurs depends on the choice of substrate. A three-dimensional growth morphology can also develop for kinetic reasons, either during $c\perp$ growth once threading dislocations are present, or at higher supersaturation when the growth mode switches to $a\perp$.

2. Experimental

The *Z*-contrast technique provides an incoherent image combining direct atomic resolution with "column-by-column" compositional sensitivity [9,10]. The objective lens of the microscope is located before the specimen and used to form a finely focused

[1] Also at the Department of Physics and Astronomy, University of Tennessee, Knoxville, TN 37996, USA.

0921-4534/92/$05.00 © 1992 Elsevier Science Publishers B.V. All rights reserved.

probe which is scanned over the sample. There are no imaging lenses after the sample; instead the high-angle scattering is detected as a function of probe position and used to map the scattering power of the sample, which depends on the square of the atomic number Z. Channeling effects confine the current to the atomic columns so that, for a sufficiently small probe, the columns are illuminated one by one, and thereby revealed directly in the image. This is a dark-field technique, so that atomic columns are seen as bright spots in the image; the heaviest columns are always the brightest features, allowing the unambiguous discrimination of Ba, Pr and Y. Similarly, the Cu-chain planes always image as dark lines, due not to the lower oxygen content (O is too light to contribute significantly to the high-angle scattering), but because the Ba–Ba separation is larger than the Ba–Y separation. All Z-contrast images were obtained with a VG Microscope's HB501 UX STEM operating at 100 kV accelerating voltage and a probe size (FWHM intensity) of 2.2 Å. The plan view TEM studies were carried out using a Philips EM400 microscope.

Films and superlattices were grown by laser ablation using a KrF (248 nm) excimer laser at an energy density of $\sim 2\ \mathrm{J\,cm^{-2}}$ to give a deposition rate of approximately $1\ \mathrm{Å\,s^{-1}}$ [11]. Film surface temperatures are estimated to be 40°C lower than the heater temperatures quoted below. Growth interruptions between target changes were typically 20 s. The STM images were obtained with a Nanoscope II operating in air with 0.3 nA tunneling current and 0.5 V bias [8].

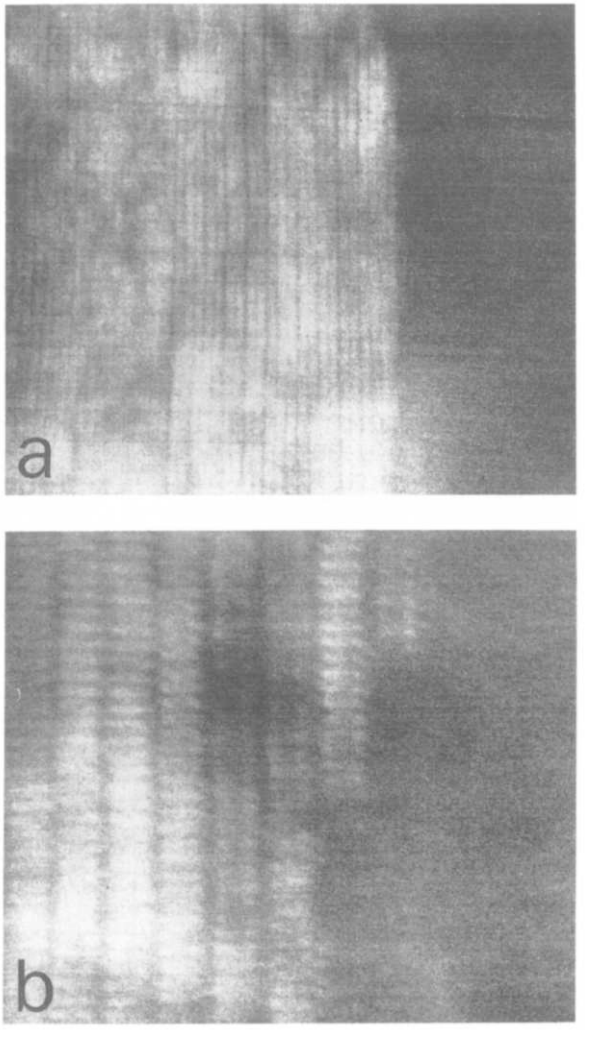

Fig. 1. Z-contrast image of an amorphous/crystal interface in $c\perp$ ion-implanted YBCO revealing the preferred crystal termination at the Cu-chain plane.

3. Cell-by-cell growth of $YBa_2Cu_3O_{7-x}$ on $SrTiO_3$

RHEED oscillations have shown the strong tendency of oxide materials to grow unit cell by unit cell when all constituents are provided simultaneously [12]. They cannot, however, indicate the crystal termination during growth, which is of major interest if attempting to fabricate planar superconducting devices. Both the origin of this behavior and the surface terminating plane can be inferred from fig. 1, which shows the amorphous/crystalline interface formed by room-temperature implantation of oxygen ions into a thin film of $YBa_2Cu_3O_{7-x}$ (YBCO). The macroscopic waviness seen in the low-magnification view is seen at higher resolution to resolve into discrete interface steps, the height of each step being the full 11.7 Å c-axis lattice parameter. Remarkably, the interface is atomically abrupt and shows an overwhelming tendency to reside at the Cu-chain planes in the crystal, which are seen as the dark vertical lines. This observation implies that the surface energy of the Cu-chain plane must be substantially lower than that of the many other possible crystal termination planes. The Cu-chain plane is

therefore the thermodynamically preferred crystal termination. This explains why the $c\perp$ growth mode is thermodynamically preferred, and why it too proceeds on a cell-by-cell basis to maintain the same low-energy terminating plane.

This interpretation assumes that, during implantation, the end-of-range region is close to thermal equilibrium. Striking evidence that this is indeed true comes from studies of Si, where it was shown that the position of the amorphous/crystal interface could be altered *reversibly* by changing incident flux or substrate temperature [13]. Thus we can consider the cell-by-cell amorphization seen in fig. 1 to represent the reverse process to the thermodynamically preferred growth mode. It should be noted, however, that fig. 1 shows only the location of the terminating plane within the unit cell. Our current image resolution is not sufficient to determine the number and arrangement of Cu atoms on this plane directly.

Images from $YBa_2Cu_3O_{7-x}/PrBa_2Cu_3O_{7-x}$ superlattices grown on $SrTiO_3$ directly confirm that $c\perp$ growth proceeds on a cell-by-cell basis. Figure 2 shows a single-unit cell superlattice in which the single YBCO layer, though stepped, is clearly seen to be almost perfectly completed before the next layer is nucleated [5]. The steps reflect the statistical nature of island nucleation and subsequent coalescence, and are uncorrelated in neighboring YBCO layers. Thus growth is occurring through the sequential nucleation and coalescence of islands, as indicated schematically in fig. 3, which is the origin of the RHEED oscillations. In addition, the lateral size of the unit cell high islands under the nonequilibrium conditions of actual growth can be inferred from the separation of steps, which is seen to be 20–30 nm.

This two-dimensional island growth mode results in a gradual roughening of the film's surface morphology with increasing film thickness. Note that the transition between step-flow growth (nucleation at preexisting surface steps) and two-dimensional island growth (nucleation on the terraces) occurs when the surface diffusion length L_D is comparable to the terrace width L_T. This is controlled by the supersaturation during growth (temperature, deposition rate, and oxygen partial pressure) and by substrate tilt.

This growth behavior has been confirmed directly by STM observations at different film thicknesses [8], which are presented in fig. 4. In the case of a

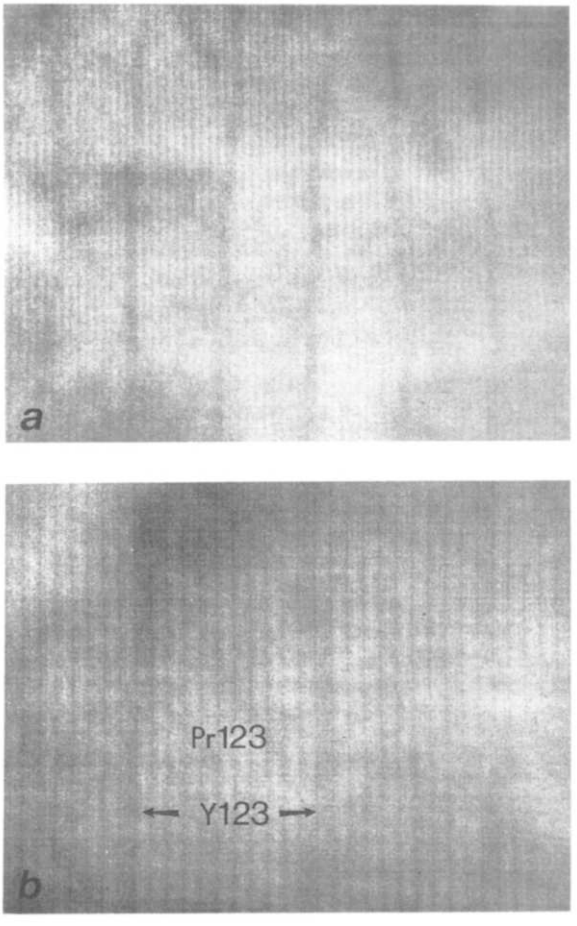

Fig. 2. Z-contrast image of a 1×8 YBCO/PBCO superlattice revealing the two-dimensional cell-by-cell growth mechanism.

$SrTiO_3$ substrate (fig. 4(a–c)), the film initially grows very smoothly, the dominant surface features being substrate steps preserved in the film's surface morphology. By a thickness of 16 unit cells, flat-topped islands are seen, in accord with the cross section images of fig. 2. It is not clear at this stage of film growth whether the roughening is due to kinetic factors or represents the onset of islanding to relieve the substrate misfit strain. (Ion channeling studies clearly show that YBCO on $SrTiO_3$ grows strained initially [14].) By a thickness of 200 nm, however, the surface morphology is very different. Large spiral-topped growth pyramids are seen, indicating that the film has now relaxed and contains threading dislocations with a screw component. On $SrTiO_3$, there-

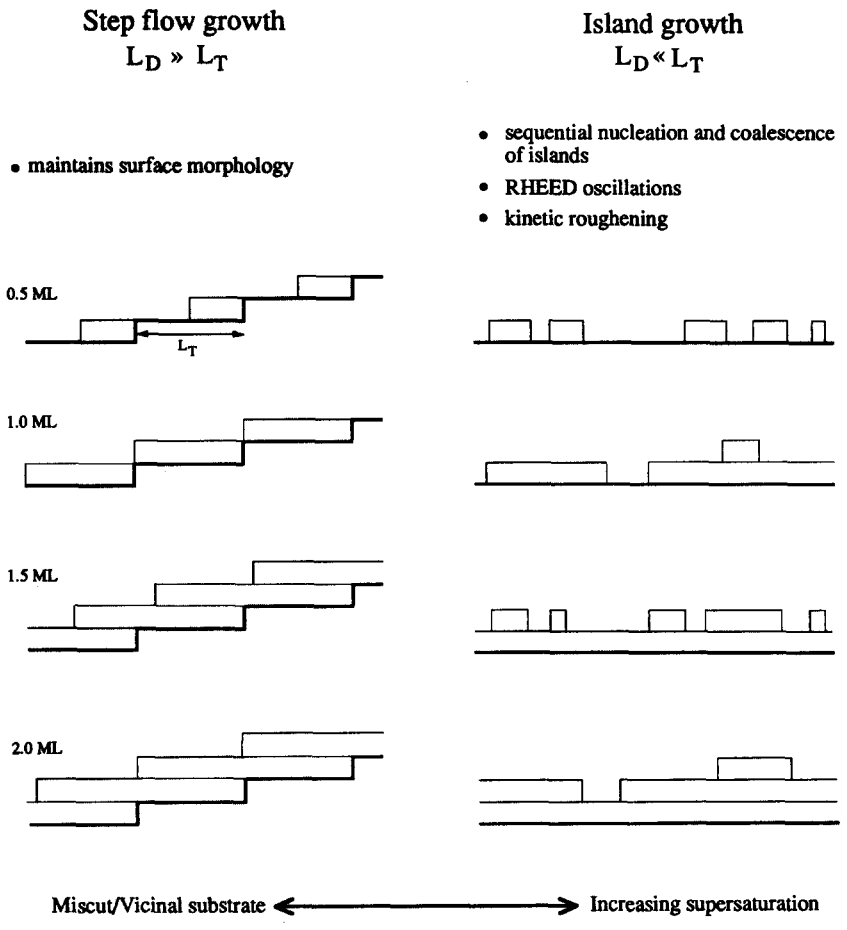

Fig. 3. Schematic indicating the transition between step-flow and two-dimensional island growth mechanisms.

fore, the growth and relaxation mechanisms appear to be those familiar from semiconductor epitaxy, with the exception that the growth unit is a complete unit cell terminated at the Cu-chain plane. The transition between terrace sweeping or two-dimensional island growth can be tuned through the deposition conditions and substrate misorientation, and relaxation occurs through a mechanism of dislocation half-loop nucleation, followed by glide to the interface to form strain relieving misfit dislocations as shown schematically in fig. 5. The dislocation segments left threading the film at each end of the misfit dislocation will have some screw component and therefore provide preferential nucleation sites where they emerge at the film's surface. This results in the growth of the large pyramids observed in thick films, a form of kinetic roughening.

Note that the density of these dislocations and the size of the pyramids will be very sensitive to the actual growth conditions. We would predict, for example, that lower deposition rates would lead to a lower density of screw segments, there being a longer time between individual nucleation events allowing more expansion of dislocation half-loops before they encounter another. This in turn will lead to a lower density of growth pyramids, and, since growth will be nearer to equilibrium conditions, their size should be smaller. Annealing a film with growth pyramids

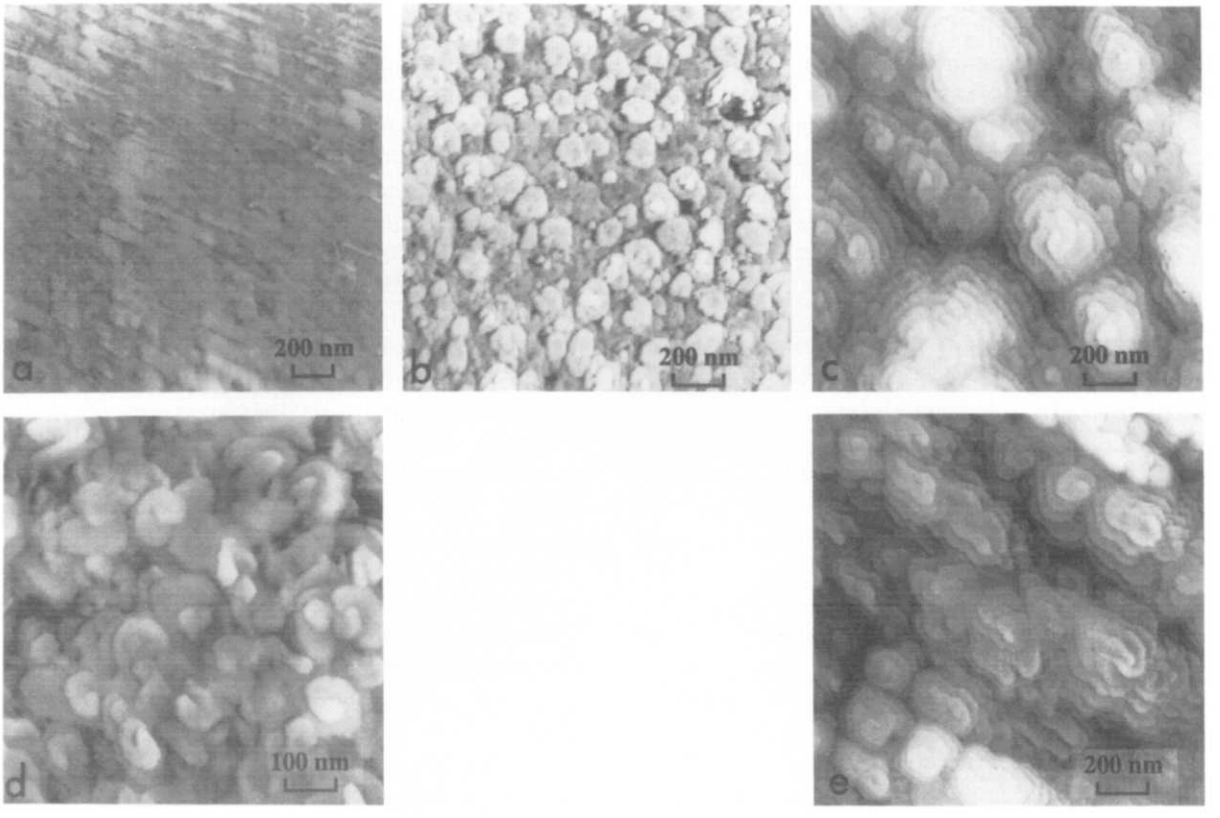

Fig. 4. STM micrographs of YBCO films deposited on $SrTiO_3$ to a thickness of (a) 8 unit cells, (b) 16 unit cells, and (c) 200 nm; and on MgO to a thickness of (d) 8 unit cells and (e) 200 nm. The early stages of growth are very different though the final microstructures are similar.

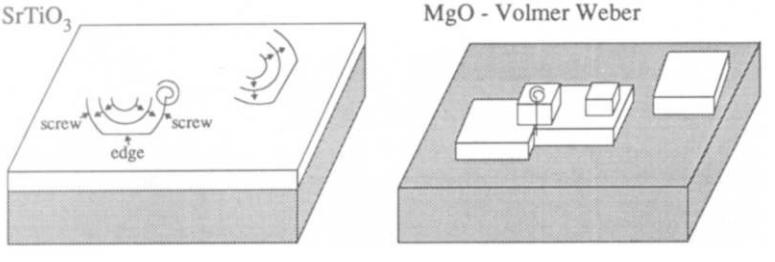

Fig. 5. Schematic showing the origin of threading dislocations (a) on $SrTiO_3$ due to strain relaxation through the surface nucleation of dislocation half-loops and (b) on MgO as a result of island coalescence.

should also result in smoothing, as the microstructure relaxes towards the thermodynamically preferred flat surface with the minimum number of steps.

4. Three-dimensional growth of $YBa_2Cu_3O_{7-x}$ on MgO

The STM image of an ultrathin film of YBCO on MgO (fig. 4(d)) shows that the initial stage of film growth is very different from growth on $SrTiO_3$. Spi-

ral-topped islands can be seen in films only a few unit cells thick. In order to distinguish Stranski–Krastanov growth (strain-driven islanding in the presence of a wetting layer of YBCO on the substrate) from Volmer–Weber growth (islanding with no wetting layer), dark-field plan view electron microscopy was performed using the {100} reflections of $YBa_2Cu_3O_{7-x}$. Since these reflections are forbidden in MgO, the bare substrate shows dark. As can be seen in fig. 6, no wetting layer is present between the islands, and in fact the image intensity is seen to be quantized corresponding to thicknesses of 1, 2, or more unit cells of $YBa_2Cu_3O_{7-x}$.

The moiré fringes visible in the image show directly that even the single-unit-cell regions of the film have relaxed close to their bulk lattice parameter. Most of the film shows no localized strain fields indicating an incommensurate interface with the substrate. Such islands are essentially floating on the substrate surface and must presumably acquire their epitaxial alignment (cube-on-cube as shown in fig. 6) by nucleating graphoepitaxially at atomic steps in the MgO substrate. This was suggested by Norton et al. [3], although their substrates had been thermally treated to form large steps many atomic layers high. Here the same effect is occurring at substrate steps which are presumably less than the 11.7 Å height of the YBCO island.

Small regions of the film, however, show fringes having twice the periodicity of the moiré fringes. This indicates the presence of interfacial dislocations, and therefore the formation of significant chemical bonding with the substrate. Their presence has been confirmed by tilting experiments as shown in fig. 7. Since the moiré fringes result from interference between beams diffracted by the film and those diffracted by the substrate, high visibility fringes only occur over a small range of incident beam orientations. On tilting the specimen slightly, the moiré fringes almost vanish while the interfacial dislocations remain in strong contrast.

Cross section images have also indicated two different forms of interface structure. In fig. 8, the light MgO substrate shows dark, and most of the interface is seen to prefer the Cu-chain terminating plane. In some areas two rows of Ba atoms are visible, which implies that the interface is formed at the CuO_2 planes. It is tempting to associate the stable Cu-chain termination with the incommensurate islands seen in plan view TEM, and the minority higher energy CuO_2 termination with the formation of interfacial bonds and localized misfit dislocation cores. Careful examination of fig. 1 also reveals some indications of this termination at the amorphous/crystal interface, implying that it is a slightly higher energy termination and therefore less common. Although detailed interface structures cannot be deduced without improved image resolution, it is clear that the existence of a single interface structure is rather unlikely, even for a single epitaxial orientation, given the number of possible structures with rather similar energies.

Individual islands tend to show small angular misalignments, and as they coalesce on further film deposition, they form low-angle grain boundaries. The edge components of grain boundary dislocations can be seen clearly in the moiré patterns. Interestingly, many small pinholes can also be seen in the film, with diameters ~ 7 nm. From the surrounding moiré fringes, it is clear that if filled they would contain a dislocation core (usually one {200} moiré fringe terminates indicating a partial dislocation). Whether or not these pinholes eventually fill, they will be capable of acting as active flux pinning sites, since the strain field around a threading dislocation can prevent the orthorhombic to tetragonal transition [15].

Islands nucleating on substrate terraces of different height could also produce $c/3$ stacking faults on coalescence. Films grown at low substrate temperatures retain such stacking faults, which run right through the film thickness (see fig. 9) [16], and seriously degrade the transport properties. The removal of this fault requires the nucleation of a screw dislocation, which, since stacking faults are not seen at normal film deposition temperatures, is presumably the origin of the high density of growth spirals observed in the early stages of film growth by STM [$\sim 10^{10}$ cm^{-2}, see fig. 4(d)]. The edge dislocation density can be determined directly from the moiré patterns and was found to be $\sim 10^{11}$ cm^{-2} (similar to that seen by Streiffer et al. [4]). The total density of threading dislocations seems quite ample to account for the strong flux pinning seen by Mannhart et al. [17]. However, their films were grown on $SrTiO_3$ and had a much lower density of screw dislocations. Based on our results, there is no obvious

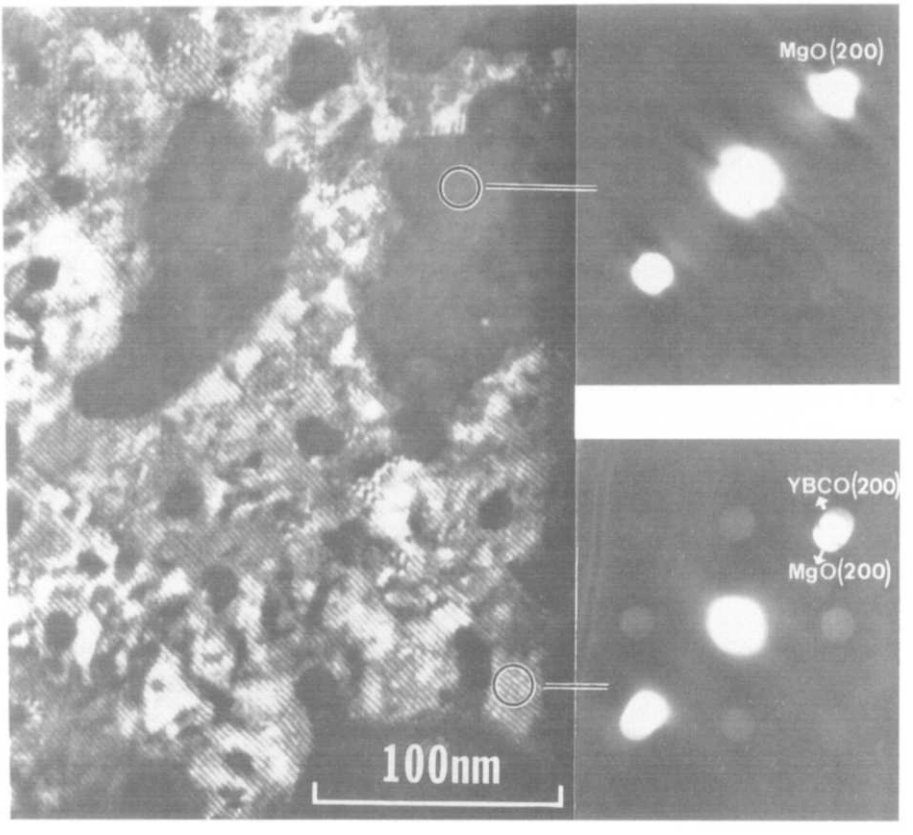

Fig. 6. Dark-field plan view TEM image and microdiffraction patterns from a three unit cell YBCO film deposited on MgO. Dark regions represent bare substrate, and moiré fringes indicate relaxation has occurred in single unit cell regions of the film.

reason for the existence of a high density of threading edge dislocations. Even though their films were deposited by sputtering, we would still anticipate two-dimensional growth of a strained layer, followed by relaxation through the nucleation of dislocation half-loops. The threading dislocation segments should all have a screw component and be visible by STM. The origin of flux pinning in this case is still unknown.

5. $a\perp$ growth at high supersaturation

Although $c\perp$ two-dimensional island growth is the thermodynamically preferred growth mode of $YBa_2Cu_3O_{7-x}$, since it maintains the lowest energy crystal termination, kinetically it is rather inefficient. A large amount of surface diffusion is required to grow a layer one unit cell in thickness. If the crystal orientation were to change to $a\perp$, then practically no surface diffusion would be necessary. The incoming flux would automatically find itself at the active crystal growth sites, as indicated schematically in fig. 10. This growth mode therefore occurs under conditions of high surface supersaturation. Figure 11 shows the transition from $c\perp$ growth near the substrate to $a\perp$ growth.

The surface morphology also changes radically with $a\perp$ growth. Since there is no long-range surface diffusion, the scale of the roughness decreases sharply. Instead of the macroscopic waviness seen with $c\perp$ growth, a microscopic roughness develops, as preserved by the $a\perp$ superlattice imaged in fig. 12. This can only be distinguished from interdiffusion in the very thin regions of the sample, so that the image is rather noisy, but the change in composition from $PrBa_2Cu_3O_{7-x}$ to $YBa_2Cu_3O_{7-x}$, and back, can just

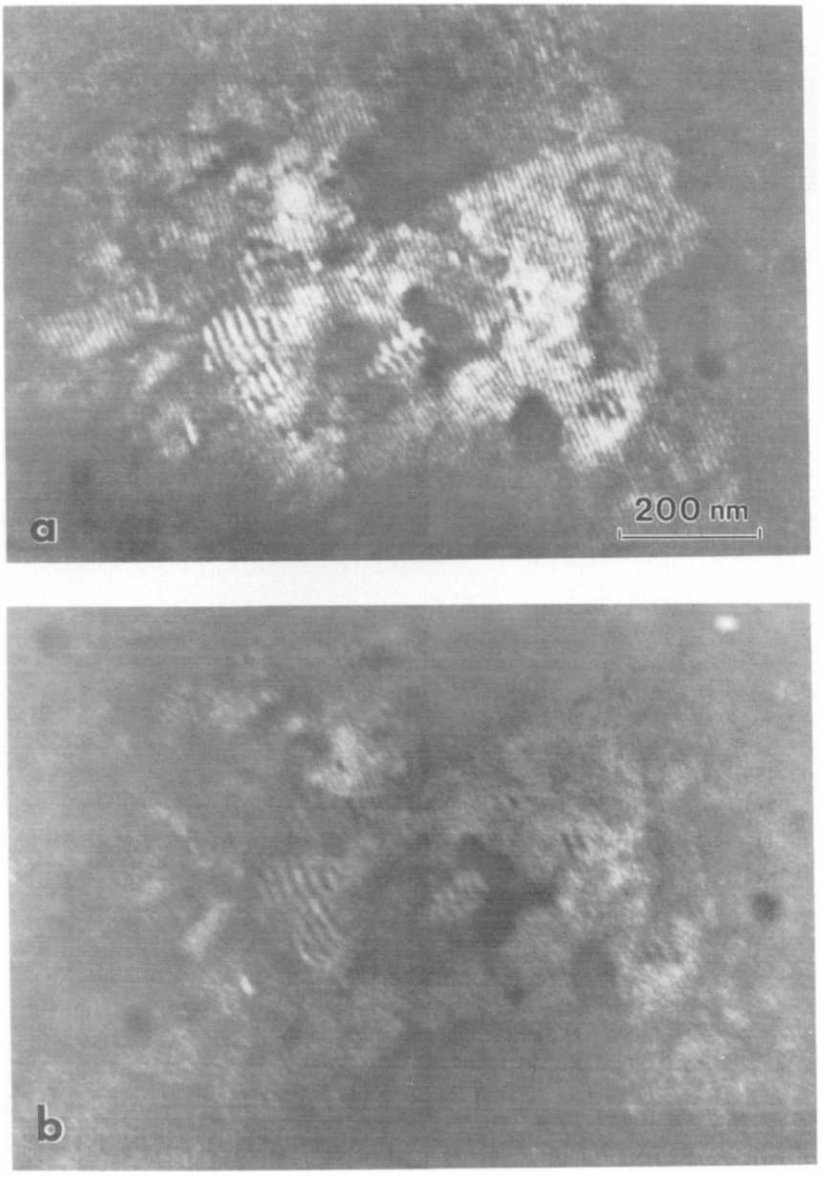

Fig. 7. (a) Image showing both moiré fringes and regions with interfacial dislocations. (b) Image after a slight tilt to reduce the visibility of the moiré fringes.

be discerned in each individual unit cell column [5].

The anisotropy in surface energies, which leads to the relatively smooth interfaces found for $c\perp$ growth (and $c\perp$ amorphization), means that there is rather little driving force for smoothing an $a\perp$ film; roughness only increases the surface area of the low-energy planes (see fig. 8). Obviously, microscopic roughness such as is seen in fig. 10 could significantly affect the characteristics of any device structure requiring thin insulating layers, particularly a tunnel junction. In view of the recent interest in such devices [18] this is a major concern, although neither diffraction contrast TEM nor STM has had the resolution to detect it. Recently, however, Matsumoto

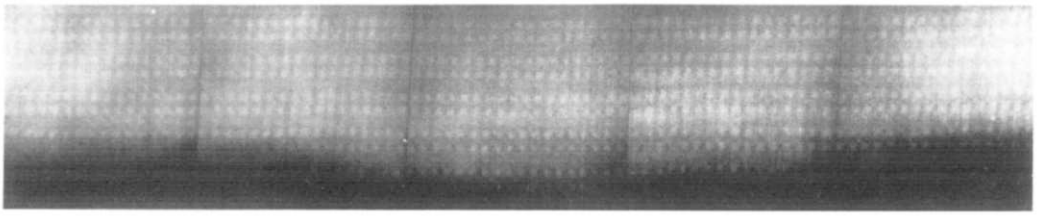

Fig. 8. Z-contrast image of MgO/YBCO interface showing two different interface structures.

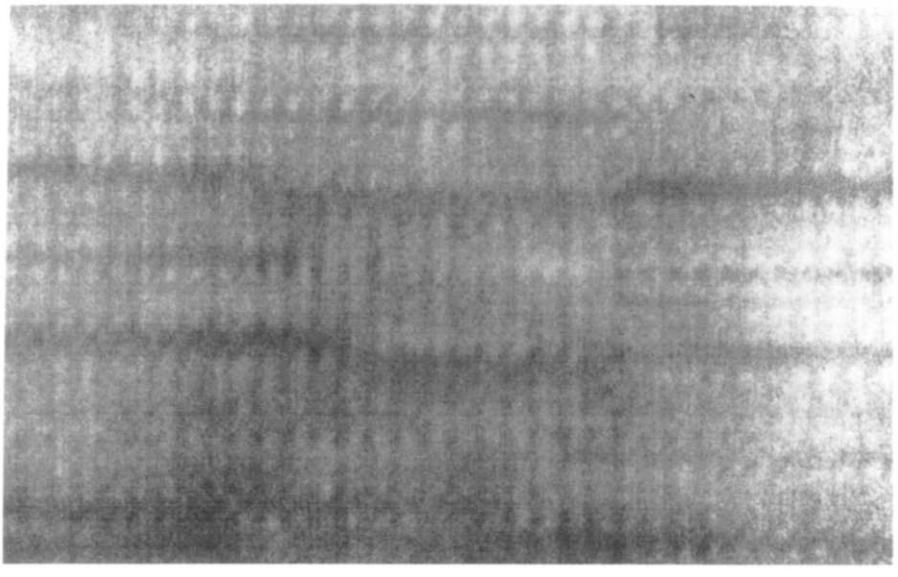

Fig. 9. $c/3$ stacking faults produced by low-temperature deposition.

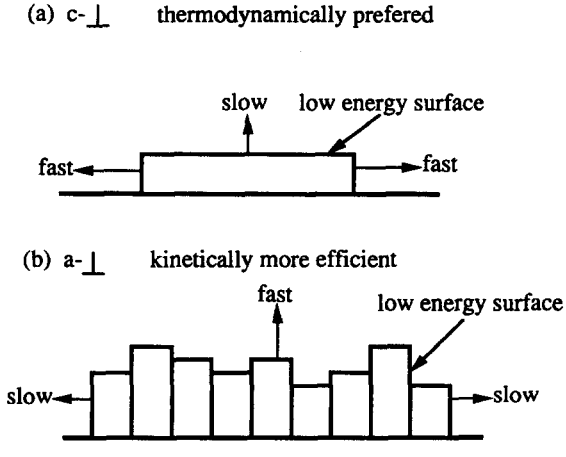

Fig. 10. Schematic indicating the transition from thermodynamically preferred $c\perp$ growth to kinetically preferred $a\perp$ growth at high supersaturation.

et al. have demonstrated [19] near-atomic resolution STM images from $SrTiO_3$ using highly doped crystals.

Note also that once the $a\perp$ morphology has nucleated, it continues through the superlattice structure in spite of growth interruptions at target changes. Streiffer et al. [20] have found $a\perp$ growth to be nucleated directly from a $LaAlO_3$ substrate. Thus, it seems likely that in this case lower deposition rates or longer growth interruptions could be used to reduce the surface roughness to desirable levels.

6. Summary

The thermodynamically preferred growth mode of YBCO is $c\perp$, maintaining the low-energy Cu-chain

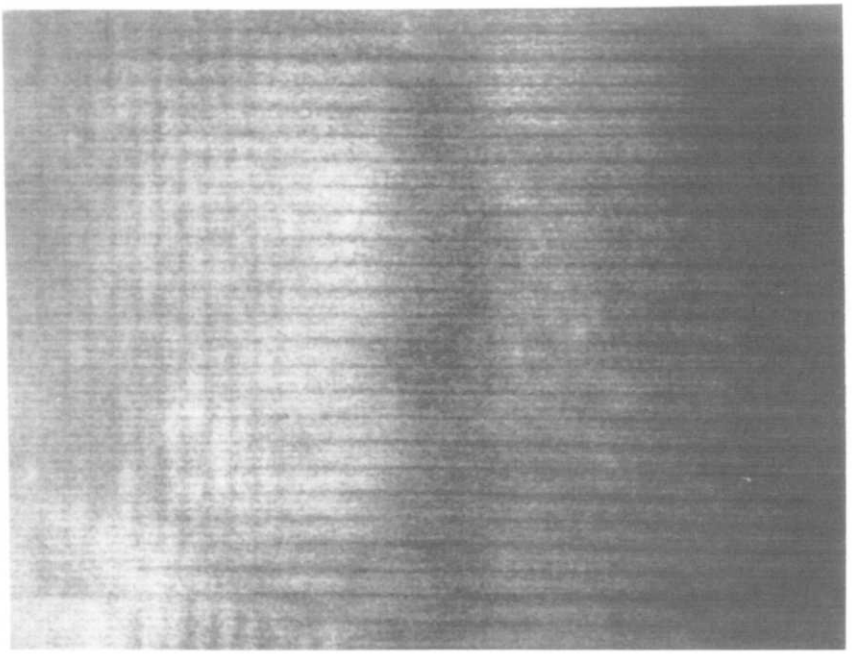

Fig. 11. Z-contrast image showing the transition from $c\perp$ to $a\perp$ growth (growth direction is towards the right).

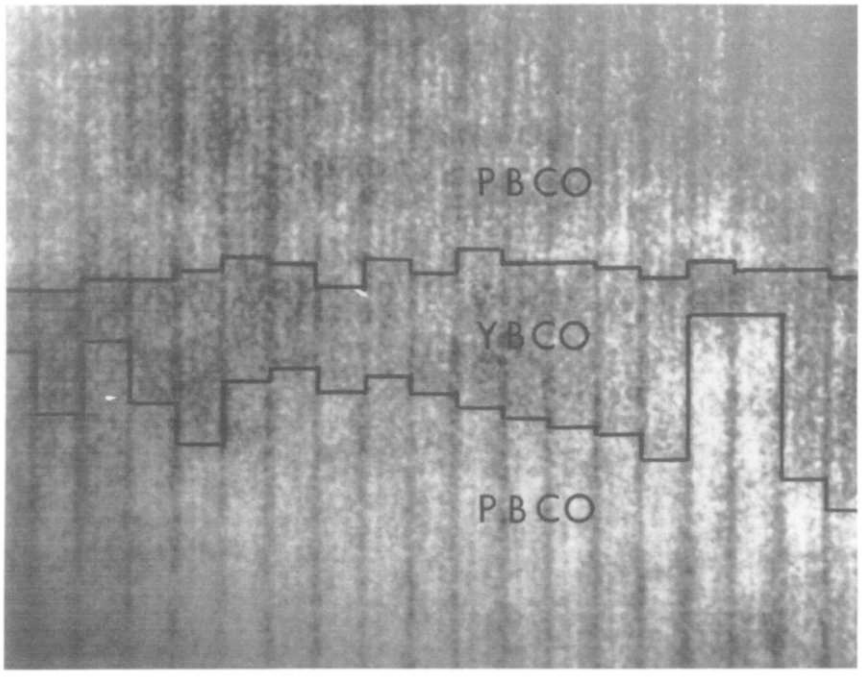

Fig. 12. Z-contrast image of an $a\perp$ 4×16 superlattice preserving remarkable microscopic interfacial roughness.

surface termination through cell-by-cell growth. The transition from step flow to two-dimensional island growth can be controlled through substrate misorientation and supersaturation. On $SrTiO_3$, films grow initially strained, and relaxation occurs through the nucleation of dislocation half-loops. The threading segments with a screw component emerging at the film surface can then act as preferential nucleation sites leading to growth pyramids. The density of threading screw dislocations is insufficient, however, to account for the strong flux pinning observed by Mannhart et al. [17], and given this growth and relaxation behavior, it is difficult to see why a high density of threading dislocations of edge character should be present.

In contrast, growth on MgO occurs by the Volmer–Weber mechanism, three-dimensional islands nucleating at atomic steps on the substrate by graphoepitaxy. Most of the interface is incommensurate with the substrate, regions only a single unit cell thick being relaxed, and small misorientations of the islands create a high density of threading dislocations as they coalesce on further deposition ($\sim 10^{11}$ cm^{-2} of edge type, 10^{10} cm^{-2} of screw type). This growth behavior does lead to the required density of threading dislocations necessary to explain strong flux pinning.

Substantial kinetic roughening has been observed for $a\perp$ growth induced through high supersaturation, as well as for $c\perp$ growth once screw dislocations are present. The lateral scale of the roughness is two orders of magnitude smaller in the case of $a\perp$ growth.

Acknowledgements

We should like to thank J.T. Luck, T.C. Estes and S. Carney for technical assistance. This research was sponsored by the Division of Materials Sciences, US Department of Energy, under contract DE-AC05-84OR21400 with Martin Marietta Energy Systems, Inc.

References

[1] C. Gerber, D. Anselmetti, J.G. Bednorz, J. Mannhart and D.G. Schlom, Nature (London) 350 (1991) 279.
[2] M. Hawley, I.D. Raistrick, J.G. Beery and R.J. Houlton, Science 251 (1991) 1587.
[3] M.G. Norton and C.B. Carter, J. Cryst. Growth 110 (1991) 64.
[4] S.K. Streiffer, B.M. Lairson, C.B. Eom, B.M. Clemens, J.C. Bravman and T.H. Geballe, Phys. Rev. B 43 (1991) 13007.
[5] S.J. Pennycook, M.F. Chisholm, D.E. Jesson, D.P. Norton, D.H. Lowndes, R. Feenstra, H.R. Kerchner and J.O. Thomson, Phys. Rev. Lett. 67 (1991) 765.
[6] D.P. Norton, D.H. Lowndes, X.-Y. Zheng, S. Zhu and R.J. Warmack, Phys. Rev. B 44 (1991) 9760.
[7] G.D. Schlom, D. Anselmetti, J.G. Bednorz, R.F. Broom, A. Catana, T. Frey, Ch. Gerber, H.-J. Güntherodt, H.P. Lang and J. Mannhart, Z. Phys. B-Condens. Matter 86 (1992) 163.
[8] S. Zhu, D.H. Lowndes, X.-Y. Zheng, D.P. Norton and R.J. Warmack, Mat. Res. Soc. Symp. Proc. 237 (1992) 541.
[9] S.J. Pennycook and D.E. Jesson, Phys. Rev. Lett. 64 (1990) 938;
idem, Ultramicroscopy 37 (1991) 14.
[10] For reviews of applications to high-T_c superconductors, see S.J. Pennycook, Anal. Chem. 64 (1992) 263A and idem, Annual Rev. Mater. Sci. 22 (1992) 171.
[11] D.H. Lowndes, D.P. Norton and J.D. Budai, Phys. Rev. Lett. 65 (1990) 1160.
[12] T. Terashima, Y. Bando, K. Iijima, K. Yamamoto, K. Hirata, K. Hayashi, K. Kamigaki and H. Terauchi, Phys. Rev. Lett. 65 (1990) 2684.
[13] J. Linnros, R.G. Elliman and W.L. Brown, J. Mater. Res. 3 (1988) 1208.
[14] J. Mannhart, D. Anselmetti, J.G. Bednorz, A. Catana, Ch. Gerber, K.A. Müller and D.G. Schlom, Z. Phys. B-Condens. Matter 86 (1992) 177.
[15] M.F. Chisholm and S.J. Pennycook, Nature (London) 351 (1991) 47.
[16] R. Ramesh, A. Inam, D.M. Hwang, T.S. Ravi, T. Sands, X.X. Xi, X.D. Wu, Q. Li, T. Venkatesan and R. Kilaas, J. Mater. Res. 6 (1991) 2264.
[17] J. Mannhart, D. Anselmetti, J.G. Bednorz, A. Catana, Ch. Gerber, K.A. Müller and D.G. Schlom, Z. Phys. B-Condens. Matter 86 (1992) 177.
[18] C.B. Eom, A.F. Marshall, J.-M. Triscone, B. Wilkens, S.S. Laderman and T.H. Geballe, Science 251 (1991) 780.
[19] T. Matsumoto, H. Tanaka, T. Kawai and S. Kawai, to be published.
[20] S.K. Streiffer et al., presented at Mater. Res. Soc. Symp. T., Spring 1992.